*Acta Oceanol. Sin.*, 2015, Vol. 34, No. 11, P. 118–125
DOI: 10.1007/s13131-015-0755-z
http://www.hyxb.org.cn
E-mail: hyxbe@263.net

# Temporal variability of vertical heat flux in the Makarov Basin during the ice camp observation in summer 2010

GUO Guijun[1, 2], SHI Jiuxin[1, 2*], JIAO Yutian[1, 2]

[1] College of Physical and Environmental Oceanography, Ocean University of China, Qingdao 266100, China

[2] Key Laboratory of Physical Oceanography, Ministry of Education, Qingdao 266003, China

Received 2 June 2014; accepted 11 June 2015



**Abstract**

Based on hydrographic data obtained at an ice camp deployed in the Makarov Basin by the 4th Chinese Arctic Research Expedition in August of 2010, temporal variability of vertical heat flux in the upper ocean of the Makarov Basin is investigated together with its impacts on sea ice melt and evolution of heat content in the remnant of winter mixed layer (rWML). The upper ocean of the Makarov Basin under sea ice is vertically stratified. Oceanic heat flux from mixed layer (ML) to ice evolves in three stages as a response to air temperature changes, fluctuating from 12.4 W/m$^2$ to the maximum 43.6 W/m$^2$. The heat transferred upward from ML can support (0.7±0.3) cm/d ice melt rate on average, and daily variability of melt rate agrees well with the observed results. Downward heat flux from ML across the base of ML is much less, only 0.87 W/m$^2$, due to enhanced stratification in the seasonal halocline under ML caused by sea ice melt, indicating that increasing solar heat entering summer ML is mainly used to melt sea ice, with a small proportion transferred downward and stored in the rWML. Heat flux from ML into rWML changes in two phases caused by abrupt air cooling with a day lag. Meanwhile, upward heat flux from Atlantic water (AW) across the base of rWML, even though obstructed by the cold halocline layer (CHL), reaches 0.18 W/m$^2$ on average with no obvious changing pattern and is also trapped by the rWML. Upward heat flux from deep AW is higher than generally supposed value near 0, as the existence of rWML enlarges the temperature gradient between surface water and CHL. Acting as a reservoir of heat transferred from both ML and AW, the increasing heat content of rWML can delay the onset of sea ice freezing.

**Key words:** sea ice, heat flux, remnant of winter mixed layer, heat content, Makarov Basin

**Citation:** Guo Guijun, Shi Jiuxin, Jiao Yutian. 2015. Temporal variability of vertical heat flux in the Makarov Basin during the ice camp observation in summer 2010. Acta Oceanologica Sinica, 34(11): 118–125, doi: 10.1007/s13131-015-0755-z

## 1 Introduction

Climate in the Arctic shows an abrupt warming tendency since the 1970s (McPhee et al., 2009), and as a response, the Arctic sea ice decreases rapidly (Comiso et al., 2008). Satellite data indicates that Arctic sea ice extent reduces at a rate of 2%–4% per decade (Stroeve et al., 2008), reaching the record minimum lower than 4×10$^6$ km$^3$ in September, 2012 (Liu and Key, 2014). However, sea ice change caused by global warming is more than concentration descending, the nature itself instead also shows an obvious change: transforming from large area of perennial ice to younger ice (Fowler et al., 2004; Maslanik et al., 2007). The area of perennial ice in the Arctic decreased to 37% of the climatological average value in 2007 (Comiso et al., 2008). The proportion of perennial ice drops from 75% in 2008 to 45% in 2011 (Maslanik et al., 2011), which results in the irreversible increasing melt of sea ice and may bring about the ice-free Arctic in summer (Lindsay et al. 2009). The maintenance of perennial ice relies on the delicate energy balance at the interface between ice and ocean, and oceanic heat flux from the ocean mixed layer to the ice plays a crucial role in the balance, which is determined by heat content in the mixed layer (ML) and turbulent mixing. Model results indicate that an ice bottom heat flux of 2 W/m$^2$ from the ML is essential for the equilibrium of 3 m ice thickness (Maykut and Untersteiner, 1971; Maykut, 1982). Solar radiation energy stored in the ML is generally suspected as the main source for ice bottom heat flux compared with the heat transferred upward from warm Atlantic water (AW) (Dewey et al., 1999; Sirevaag et al., 2011). Solar radiation heats the ML through leads, open water and melt ponds. With the seasonal evolution of sea ice extent and solar radiation, heat content in the ML shows a seasonal variability (Maykut and McPhee, 1995). The observational annual average ice bottom heat flux is around 2–4 W/m$^2$ with seasonal changes due to heat content variability in ML (McPhee et al., 2003). Before the end of melting season in August, maximum of the heat flux to ice reached 40–60 W/m$^2$ (Maykut and McPhee, 1995). Krishfield and Perovich (2005) found that ice bottom heat flux has a long-term increasing tendency at a rate of 0.2 W/m$^2$ per decade in 1975–1998 and a positive heat flux to the ice was not negligible in winter, suggesting other heat sources for the ice besides solar energy. Heat from deep warm AW might be a possible source for winter surface water heat flux to the ice and might have a larger effect on the upper ocean than generally suspected. With the extent and thickness decreasing in the Arctic, a better understanding of the ice bottom heat flux from ML and its heat sources and impacts on sea ice melt is necessary due to its key role in maintaining the equilibrium of sea ice.

Foundation item: The Global Change Research Program of China under contract No. 2015CB953902; the National Natural Science Foundation of China under contract Nos 41330960 and 40976111.

*Corresponding author, E-mail: shijiuxin@ouc.edu.cn

Part of solar heat energy entering the Arctic ML in summer is transported upward to melt ice, and part of the rest downwells across the base of ML through turbulent diffusivity. In Makarov Basin, the remnant of winter mixed layer (rWML, Fig. 1) lies beneath the ML characterized by local temperature minimum. The temperature of rWML is generally near freezing point (Rudels et al., 1996), which results from the extreme surface cooling and enhanced deep convection during sea ice formation in winter. The temperature gradient between ML and rWML makes it possible that heat in ML fluxes downward and is reserved in the rWML. Blow the rWML resides the cold halocline layer (CHL) with strong stratification, which performs as an efficient barrier between the surface mixed layer and warm salty AW (Aagaard et al., 1981). Generally, strong stratification and relatively low temperature gradient of CHL can effectively hinder the upward heat transport from warm AW below (Rudels et al., 1996; Steele and

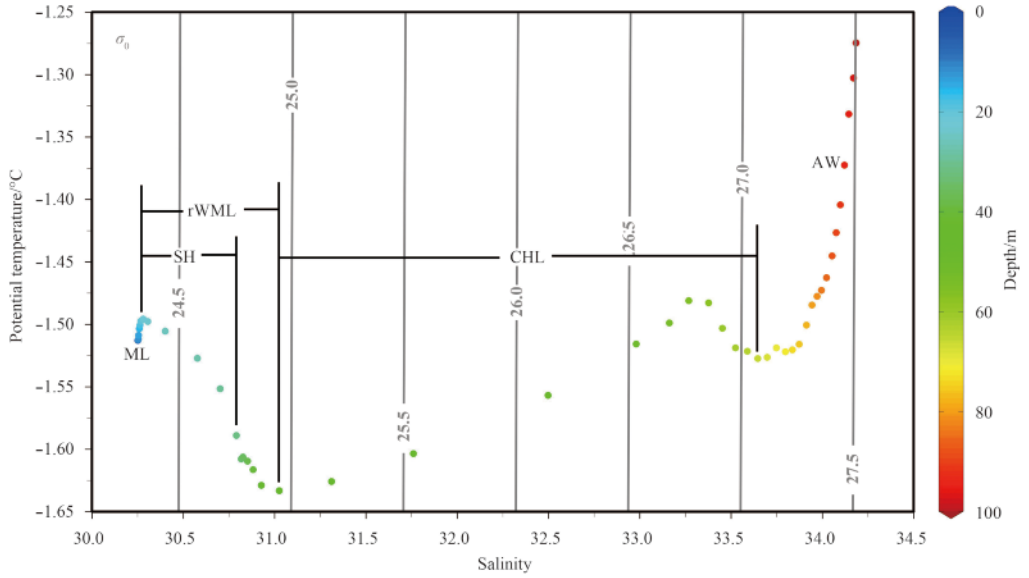


**Fig. 1.** Temperature-salinity diagram for the upper 100 m under sea ice. Data was from CTD profiles obtained at the ice camp deployed in the Makarov Basin during the 4th Chinese Arctic Expedition in 2010.

Boyd, 1998) and the observational result of heat flux from AW through CHL is near zero in Amundsen Basin (Fer, 2009). However, Krishfield and Perovich (2005) found the unnegligible heat flux from ML to the ice in winter and the potential heat source for the winter ML might be the vertical heat flux from warm AW. The existence of near freezing rWML in summer creates a comparable vertical thermohaline structure similar to that in winter and can enlarge the temperature gradient between surface water and CHL, indicating a relatively larger quantity of heat from AW can be transferred upward through CHL and stored in rWML. Therefore, the significance the rWML carries should be clarified in the study of upward heat flux from AW.

For a better understanding of heat flux from the ML to sea ice and the reservoir effects of rWML for heat through vertical heat flux from both ML and deep AW, we investigate the thermal dynamics of the ice-covered upper ocean, based on the conductivity, temperature and depth (CTD) profiles, Acoustic Doppler Current Profiler (ADCP) data sets together with drifting GPS and air temperature data, collected at an ice camp deployed by the 4th Chinese Arctic Research Expedition in 2010. In the next section the data analyzed in this paper and the processing procedures are presented. In Section 3, vertical thermohaline structures in the upper ocean under sea ice in Makarov Basin and its temporal variability are described. In Section 4, ice bottom heat flux from ML and its effects on sea ice melt are discussed. Heat flux across the top and base interfaces of rWML and the heat content evolution of rWML are estimated to examine the reservoir effects for heat in Section 5. A summary is given in Section 6.

## 2 Data and processing

The ice camp was deployed by the 4th Chinese Arctic Research Expedition during 8–19 August, 2010 (Fig. 2). Kawaguchi et al. (2012) found a significant reduction of sea ice concentration in the central basin in the mid-August, during which our ice camp was deployed. Sea ice reduction can increase absorption of solar radiation in surface water, resulting in aggravated sea ice melt. The starting location of the ice camp was at 86.884°N, 179.162°W in the Makarov Basin. Before 16 August, the ice drift was dominantly westward and then turned to north, with an average speed of 17 cm/s. CTD profiles were collected with an XR-620 self-contained CTD (RBR Ltd, Canada) which was deployed through an ice hole by a programmed winch twice a day, sampling the upper 100 m ocean under sea ice at 6 Hz. Considering the safety of CTD, not all the profiles started from surface level. Water speed relative to the ice was recorded by a 300 kHz ADCP hanged in the water at 3 m depth, which was set to sample 6 minute ensembles with 2 m bins. As the first bin data recorded by ADCP is generally lack of good quality (Thurnherr, 2008), the second bin centered at 9 m to the 34th bin centered at 73 m were used for analysis. As the mixed layer extends about 25 m (Section 3), lack of surface CTD and ADCP data carries no obvious effect on the analysis of heat flux below sea ice. GPS data and air temperature at 10 m level were also analyzed in this paper, sampled every 10 min during the observation.

The ice camp drifted in a relatively small area, so discussion about heat content and heat flux in the following sections do not represent the tendency of the entire basin, but it can still shows

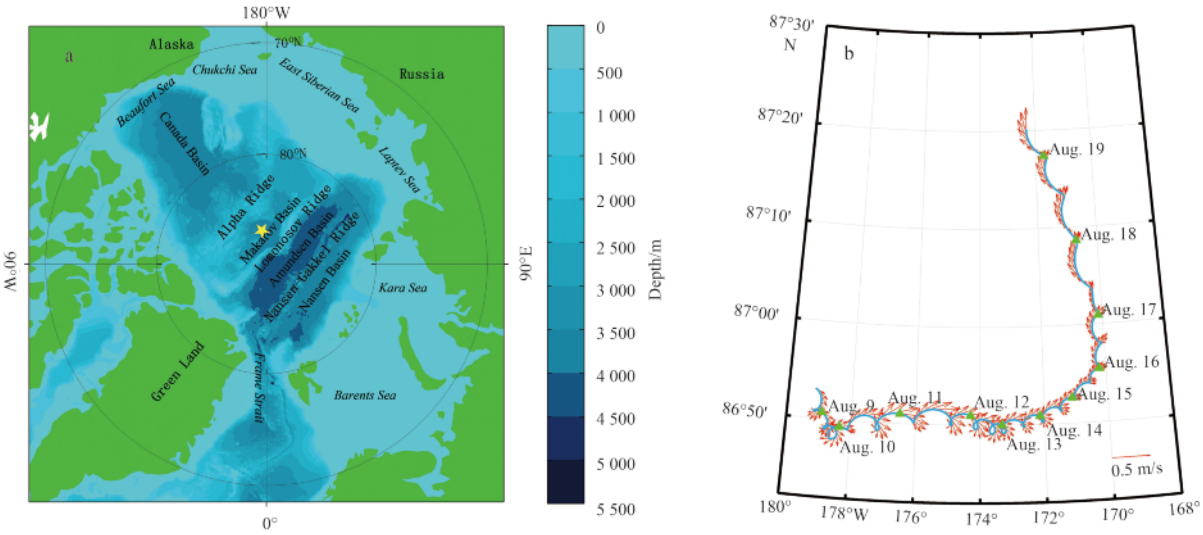


**Fig. 2.** Bathymetric map of the Arctic Ocean and central location of the ice camp (designated by yellow pentagram) (a); and trajectory of the ice camp (b), the starting location of the ice camp for each day is designated by green triangles, hourly mean drifting velocity by red arrows.

the local changes of heat content and heat flux where the ice camp drifts and illustrates their impacts on local environment.

### 2.1 *Estimate for ice bottom heat flux*

Ice bottom heat flux from ML water $F_{h_0}$ is given by

$$F_{h_0} = \rho c_p \langle w'T' \rangle , \tag{1}$$

where  is water density, $c_p$ is specific heat of sea water, $\langle w'T' \rangle$ is vertical turbulent heat flux. McPhee (1992), McPhee et al. (1999) found that turbulent heat flux can be estimated from ice bottom interfacial friction velocity $u_{*0}$ and ML temperature above freezing point $T$, then Eq. (1) can be expressed as

$$F_{h_0} = \rho c_p c_h u_{*0} \delta T, \tag{2}$$

where $c_h$ = 0.005 7 is the bulk heat transfer coefficient (McPhee, 1992; McPhee, 2002). The $u_{*0}$ can be estimated from the difference between ice drift speed $\boldsymbol{V}_i$ and the surface geostrophic flow $\boldsymbol{V}_g$ (McPhee et al., 1999):

$$\frac{\kappa \boldsymbol{V}}{\boldsymbol{u}_{*0}} = \log \frac{u_{*0}}{f z_0} - A - \mathrm{i}B , \tag{3}$$

where $\boldsymbol{V}$= $\boldsymbol{V}_i$–$\boldsymbol{V}_g$ (2-d vector $\boldsymbol{V}$ is expressed as boldface complex number, and so is $\boldsymbol{u}_{*0}$),  is von Karman's constant with the value 0.4, $f$ is the Coriolis parameter, $z_0$ is the hydraulic roughness of the ice bottom interface with a representative value 0.01 m for the type of multiyear ice on which drifted ice camp are sited, $A$ and $B$ are constant with their respective value 2.12 and 1.91. For short time scales associated with strong wind influence, ice drift velocity usually far exceeds the surface geostrophic flow, so here $\boldsymbol{V}$ was assumed to be the actual ice drift speed $\boldsymbol{V}_i$ derived from GPS data (McPhee et al., 2003). McPhee (1988) considered that the ice velocity includes an inertial component, and the inertial period at the ice camp location is about 12 h. Hence, the daily average $\boldsymbol{V}$ was applied to evaluate $u_{*0}$ so as to eliminate the impacts of inertial flow.

### 2.2 *Heat flux calculation between different water masses*

Vertical heat flux in the ocean at the interface between different water masses can be evaluated with the CTD and ADCP data series. CTD data were firstly used to estimate the buoyancy frequency squared $N^2$:

$$N^2 = -\frac{g}{\rho}\frac{\partial \sigma_t}{\partial z} , \tag{4}$$

where $g$ is the gravity acceleration, $\frac{\partial \sigma_t}{\partial z}$ means the vertical gradient of potential density. $N^2$ is a measure of stratification and will reach the maximum value when potential density changes most fiercely. CTD profiles were averaged over 2 m so as to coincide with the ADCP's 2 m vertical bins, which were combined to acquire vertical diffusivity coefficient.

ADCP data were applied to measure vertical shear:

$$S^2 = \left(\frac{\partial u}{\partial z}\right)^2 + \left(\frac{\partial v}{\partial z}\right)^2 , \tag{5}$$

where $u$, $v$ represent east and north velocity components respectively. $S^2$ was calculated from 9 m extending downward 73 m.

The vertical diffusivity $K$ can be estimated based on PP parameterization (Pacanowski and Philander, 1981) with the combination of daily mean $N^2$ and $S^2$:

$$K = \frac{5 \times 10^{-3} + 10^{-4}(1 + 5Ri)^2}{(1 + 5Ri)^3} + 10^{-5}, \tag{6}$$

where $Ri = N^2/S^2$ represents Richardson number gradient. PP parameterization results suggest that vertical diffusivity usually occurs accompanied with weak stratification or strong vertical shear. With the vertical diffusivity $K$, heat flux across an inner ocean interface $F_h$ then can be given with the obtained daily average temperature gradient $\frac{\partial T}{\partial z}$:

$$F_h = \rho c_p K \frac{\partial T}{\partial z} . \tag{7}$$

Heat flux across an interface was calculated from 4 m above the interface down to 4 m blow.

### 2.3 *Heat content in the ocean*

Based on temperature and salinity profiles, heat content at a given depth is expressed as:

$$H = (T - T_f)\,\rho c_p, \tag{8}$$

where $T$ and $T_f$ are sea water temperature and freezing temperature. Then heat content in a given layer can be calculated from:

$$HC = \int_{z_1}^{z_2} H(z)\,\mathrm{d}z, \tag{9}$$

where $z_1$, $z_2$ are the top and base depth of the given layer in the ocean.

## 3 Thermohaline structures in the upper ocean

Figure 3 shows four daily average temperature and salinity profiles of the upper 0–100 m ocean in Makarov Basin during the ice camp observation. Below the ice resides the surface ML with a relative vertically uniform temperature and salinity. The base of ML is determined by the depth where the density gradient increases to 0.02 kg/m$^4$. For 9 to 18 August during which the measurement was conducted, the mean depth of ML is approximate 25 m, with average temperature of –1.51°C and salinity of 30.22. The rWML resides blow the ML extending downward to about 40 m, bounded by the temperature minimum of about –1.60°C. Sea ice melt in summer decreases salinity of surface ML and brings about a relatively weak seasonal halocline under the base of ML. Blow the temperature minimum, a layer with low temperature and distinct salinity gradient composes the upper CHL, which extends downward to about 70–80 m. Below CHL is AW, of which the temperature increases rapidly with a relatively moderate salinity rising.

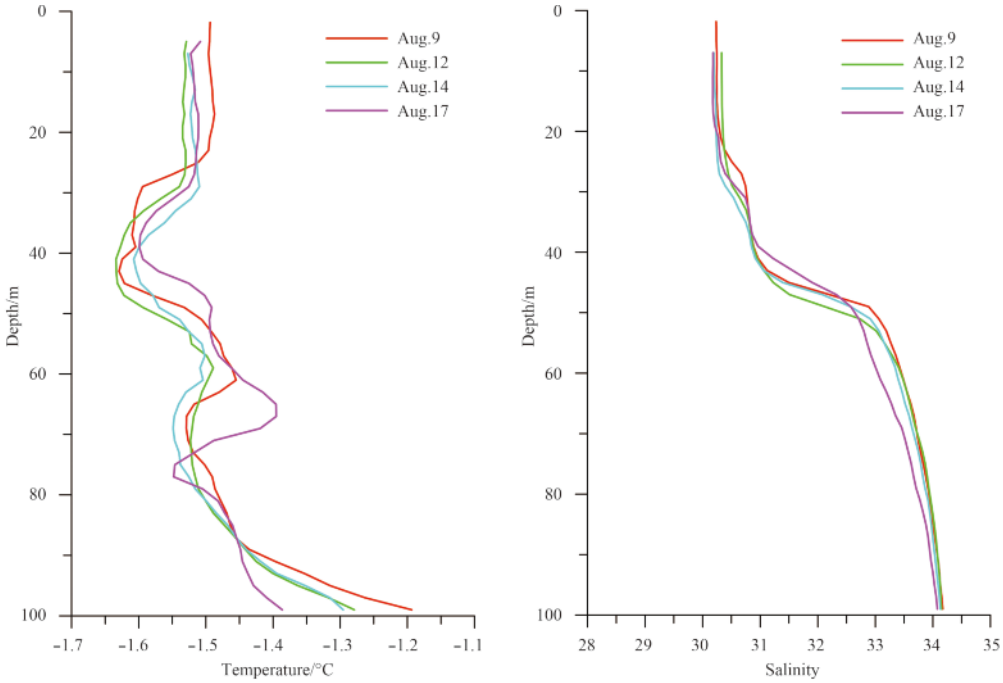


**Fig. 3.** Temperature and salinity profiles in the upper 100 m under sea ice.

Figure 4a shows the air temperature changes during the observation on ice camp. Air temperature can influence heat content in the upper ocean through leads, open water and melt ponds. Air temperature is maintained at lower than 0°C before 13 August on which an abrupt temperature decreasing occurred and reaches the minimum of –4.60°C on 16 August. Temperature change in ML is in coincidence with air temperature due to the direct interaction between atmosphere and surface water. A slight cooling of surface ML follows the drop in air temperature from 13 August but ML then turns to be warming due to rapid rising of air temperature started from 16 August (Fig. 4b). In addition, salinity in ML shows a decreasing tendency during the conduction of ice camp observation, with a lower value than 30.20 since 15 August (Fig. 4b). Ice melt freshwater is stored mainly in the surface ML and so salinity of rWML residing blow ML has no obvious changes. However, solar energy absorbed by surface water can be transferred downward, causing a warming tendency in rWML, which we will discuss in details in Section 5.

## 4 Heat flux variability from ML to sea ice

Ice speed vectors in Fig. 2b indicate an inertial component with the period of about 12 h. The daily average ice speed is used to remove the impacts of inertial flow on the estimate of heat flux from surface water to the ice. Figure 5a describes changes of daily average ice speed $V$, ice bottom interface friction velocity $u_{*_0}$ and elevation of ML temperature above freezing $T$ from 9 to 18 August. The ice drifts at a speed between 5–20 cm/s and accelerates after the direction changed from eastward to dominantly northward. The derived friction velocity $u_{*_0}$ changes similarly to $V$, with the mean value of 0.69 cm/s. Temperature and salinity at 9 m depth are adopted to designate ML, and $T$ ranges from 0.10°C to 0.17°C with the mean value 0.13°C.

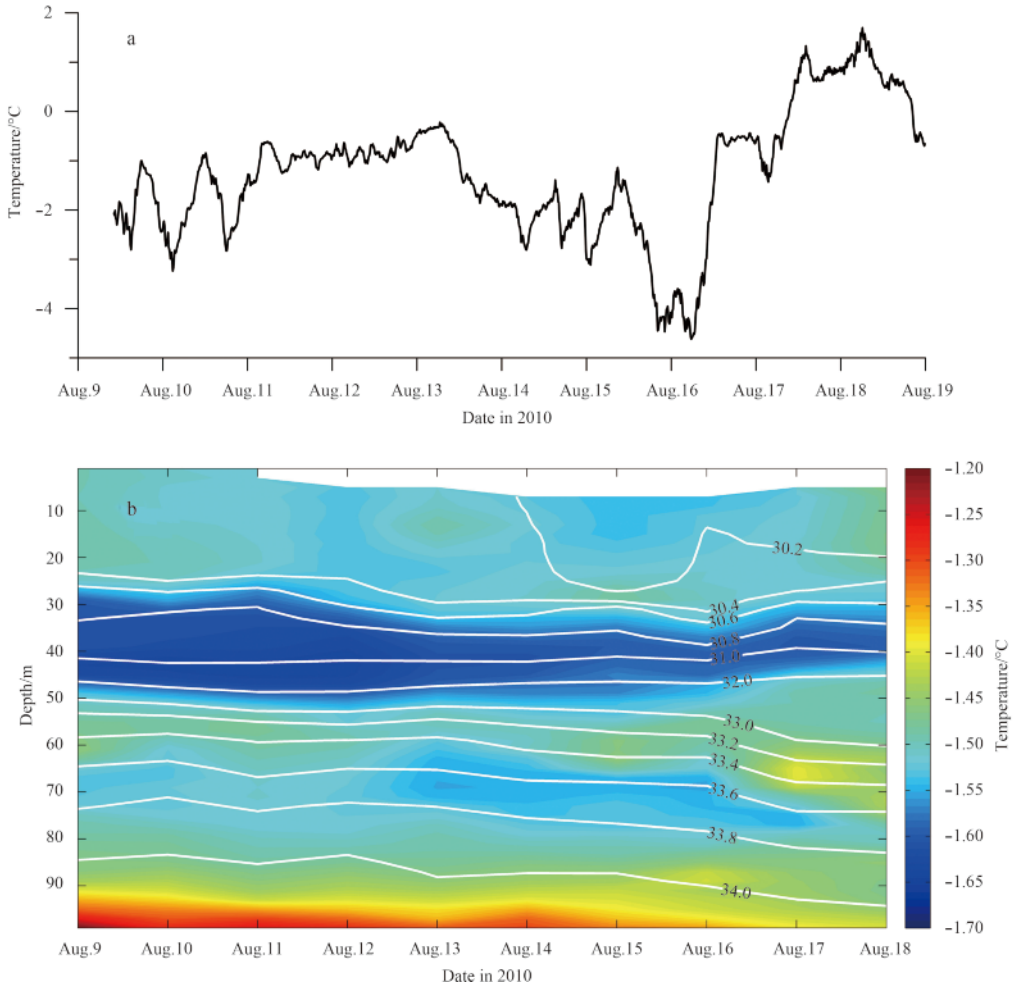


**Fig. 4.** Air temperature at 10 m level (a); temperature (colored contours) and salinity (white contours) in the upper 100 m under sea ice (b).

Combining $u_{*0}$ and $T$ with other parameters derived from temperature and salinity profiles, applying Eq. (2), evolution of ice bottom heat flux from ML to ice, $F_{h0}$, is acquired (Fig. 5b). During the ten days of the observation, $F_{h0}$ is maintained higher than 10 W/m$^2$, with the average value of 21.9 W/m$^2$, which would affect sea ice melt significantly. $F_{h0}$ evolves in three stages: a moderate ascending from 12.4 W/m$^2$ to 29.8 W/m$^2$ in the earlier three days, staying at a low level blow 15 W/m$^2$ since 12 August and a rapid rising after drift direction changing on 16 August with increasing $u_{*0}$ and $T$. On 18 August, the heat flux across the ice-ocean interface reaches the maximum of 43.6 W/m$^2$ that is coincide with the maximum range of ice bottom heat flux in August, 40–60 W/m$^2$ evaluated by Maykut and McPhee (1995).

Oceanic heat flux from ML to the ice is the major heat source for ice melt, while heat flux through conduction is negligible relative to turbulent heat flux at the ice bottom interface. The oceanic heat flux to the ice is averaged at 21.92 W/m$^2$, transferring $2\times10^7$ J/m$^2$ heat upward from ML during the ten days of observation. Assuming the heat transferred to the ice is completely used to melt sea ice, the ice bottom ablation due to melt should be $\Delta h_i = \Delta Q/\rho_i L_i$ (Steele et al., 2008), where $L_i$ =$3\times10^5$ J/kg, is sea ice latent heat of fusion, and $_i$ is sea ice density. The observed sea ice density measured by Lei et al. (2012) at the same place is about 850 kg/m$^3$. Then sea ice melt is estimated at the value of 7.4 cm due to upward heat flux from ML, with the mean ice melt rate (0.7±0.3) cm/d (Fig. 5a), slightly higher than the mean observed melt rate conducted by Lei et al. (2012), which may be caused by high frequency changes of air temperature and small temperature difference between sea surface and 9 m depth. Sea ice melt rate changes correspondingly to the ice bottom heat flux, and showes the same three evolution stages during the observation, which complies well with the observed ice bottom ablation rate changes given by Lei et al. (2012).

## 5 Energy budget and heat content evolution for rWML

Other than the part transferred upward to melt sea ice, solar heat entering surface ML during sea ice melt season can also be transferred into rWML through turbulent diffusivity. As the temperature in ML is higher than that of rWML due to solar heating in summer, a positive temperature gradient exists at the interface between ML and rWML, making a dominant downward heat flux from ML into rWML. Hence heat reserved in rWML cannot be transferred upward to melt ice directly in summer. Instead it can play a role in delaying the onset of sea ice freezing. For a better understanding of heat budget for rWML, heat flux across the top and bottom boundary is evaluated.

Based on the observational CTD and ADCP data, the buoyancy frequency and vertical shear profiles are derived. Then the

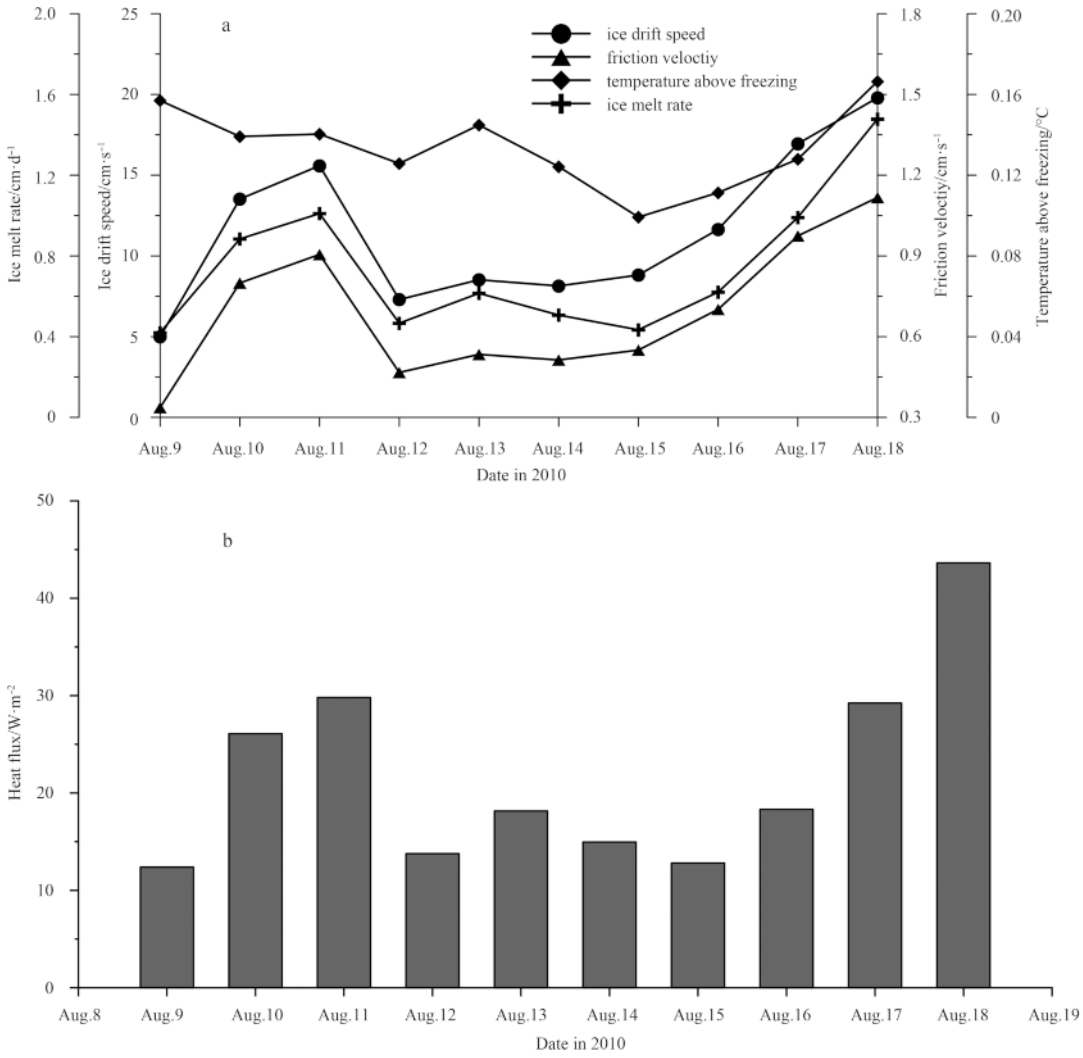


**Fig. 5.** Daily meaning ice drift speed, friction velocity under sea ice, mixed layer temperature above freezing point and ice melt rate (a); heat flux from ocean ML to ice (b).

vertical diffusivity $K$ is estimated using PP parameterization. On the top of rWML, i.e., the base of surface ML, the mean value of $K$ is $6.8\times10^{-5}$ m$^2$/s while on the bottom of rWML identified by the temperature minimum, $K$ is averaged at $1.2\times10^{-5}$ m$^2$/s. With the vertical temperature gradient heat flux across the top and bottom of rWML is given in Fig. 6a.

Heat content increasing in ML due to solar heating creates a positive temperature gradient on the interface between ML and rWML which results in a successive downward heat flux in to rWML (Fig. 6a). Compared with the upward heat flux from ML to sea ice, heat flux across the top of rWML is relatively small maintained at lower than 1.5 W/m$^2$. We conclude that solar heating in the ML in summer is mainly consumed by upward heat flux for sea ice melt with a much smaller proportion transferred downward. We infer from Fig. 6a that heat flux across the base of ML evolves in two phases due to the abrupt drop in air temperature: before 14 August, downward heat flux from ML is generally larger than 0.8 W/m$^2$ with the mean value of 1.18 W/m$^2$, whereas the mean heat flux from ML into rWML is only 0.56 W/m$^2$ since 14 August. Heat flux across the top rWML is affected directly by heat content in ML, and shows a day lag after the air temperature changes which supplies energy for ML. The relatively low downward heat flux from ML is caused by enhanced stratification in the seasonal halocline between ML and rWML due to sea ice melt. As for heat flux across the bottom rWML, Fig. 6a indicates an overall positive value except that on 12 August, which may be caused by advective heat transport resulting in a reversed temperature gradient. The mean positive heat flux into rWML from downside is 0.18 W/m$^2$, a less remarkable level relative to that from ML, indicating the barrier role of CHL for heat transferred between deep warm AW and rWML in summer. However, the mean heat flux from AW through CHL into rWML is still notable compared with the previous estimate value near 0 due to the enlarged temperature gradient. The existence of rWML magnifies heat transferred from deep AW, but the upwelling heat from AW cannot reach the surface as the heat flux across the top of rWML is dominantly downward. Heat transferred from warm AW is trapped by the rWML and has no direct effect on sea ice melt. However, working as a reservoir for heat in summer, it can delay the onset of freezing because the heat stored in rWML need to be consumed completely before freezing season begin. As the surface ML water is warming and freshening for the long run, enhanced stratification of the upper ocean can benefit the maintaining of rWML and the upward heat flux from AW is suspected

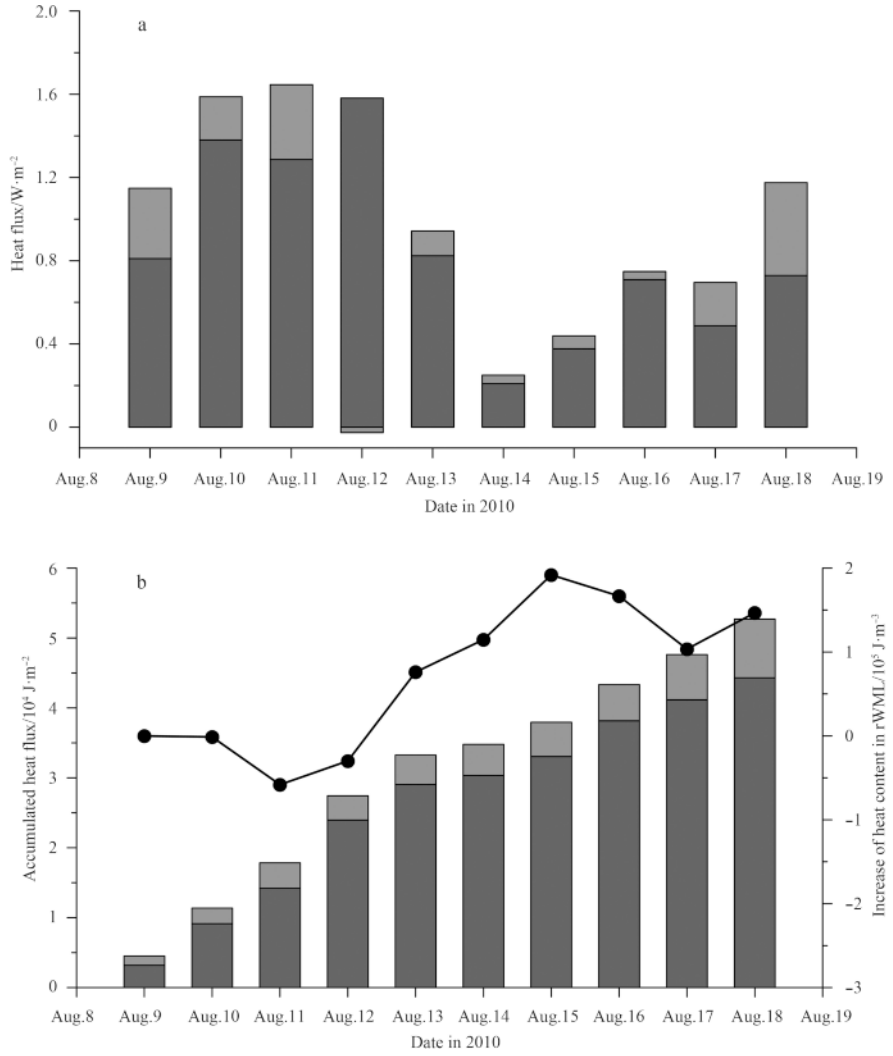


**Fig. 6.** Heat flux across the top (dark gray bars) and base (light gray bars) of rWML (with heat flux into rWML as the positive value) (a); heat budget and heat content variability rWML (b), dark gray bars denote accumulated heat transferred to rWML across the base of summer mixed layer, light gray bars denote that across the base of rWML (left axis); black dots represent change in heat content of rWML relative to that on 9 August standardized by thickness of rWML (right axis).

to increase with rapid sea ice retreat.

Continuous heat flux across the top and bottom of rWML brings about heat content variability in rWML. The curve in Fig. 6b describes heat content differences relative to the beginning day of observation standardized by thickness. Heat content in rWML tends to be ascending during the observation. On 9 August, heat content for rWML is $5.64\times10^5$ J/m$^3$, but on the ending day heat content for rWML has increased by $1.47\times10^5$ J/m$^3$, despite of a slight decrease occurs on 11 and 12 in this month. Bars in Fig. 6b denote accumulated heat transferred into rWML across its top and bottom respectively since 9 August. By the end of the measurement, accumulated heat transferred to rWML from ML is $4.43\times10^4$ J/m$^3$, while deep AW total upwelling heat is $8.39\times10^3$ J/m$^3$. Heat content increasing in rWML due to solely vertical heat flux comprises 36% of the total observed rWML heat content changes, suggesting that heat trapped in rWML from both ML and AW through vertical heat flux cannot be negligible for its role in delaying the onset of sea ice freezing season, although it does not participate in melting ice directly in summer. The other part of heat content changes can be caused by either spatial changes due to drift or advective heat transport.

## 6 Summary and conclusions

Based on hydrographic data collected at an ice camp deployed by the 4th Chinese Arctic Expedition in 2010, thermohaline structure of the upper ocean in Makarov Basin and vertical heat flux at the ice-ocean interface together with its impact on sea ice melt are discussed. Heat flux into rWML and its reservoir role in storing heat from both ML and AW are also explored.

During the observation, the well mixed layer in the Makarov Basin is about 25 m with a mean temperature of –1.51°C and salinity of 30.22. Blow ML, rWML characterized by temperature minimum of about –1.60°C extends to about 40 m. CHL residing below rWML shows large salinity gradient and strong stratification, extending to 70–80 m. Temperature of ML shows a fluctuation similar to the air temperature while salinity of ML tends to be decreasing due to sea ice melt. A warming tendency is found in rWML during the observation.

Daily mean sea ice drift speed ranges from 5 to 20 cm/s and is used to calculate the ice-bottom interface friction velocity, $u_{*0}$.

Mean surface ML water temperature above freezing, $\delta T$ is about 0.13°C, ranging from 0.10°C to 0.17°C. With the combination of $u_{*0}$ and $\delta T$, evolution of heat flux from ML to sea ice exhibits three stages with the mean value 21.9 W/m$^2$: a moderate ascending from 12.4 W/m$^2$ to 29.8 W/m$^2$ in the earlier three days, staying at a low level blow 15 W/m$^2$ from 12 to 15 August and a rapid rising after drift direction changing on 16 August. As much as 7.4 cm sea ice can be melt assuming that total heat transferred to ice from ML is completely used to melt ice during the 10 d. Sea ice melt rate is (0.7±0.3) cm/d, and changes in the same stages with ice bottom heat flux, which complies well with the observed changes of ice bottom ablation rate given by Lei et al. (2012).

Beside the heat transferred upward to sea ice, solar heat entering surface ML can also be transferred downward and stored in rWML. Turbulent diffusivity at the top and bottom of rWML is $6.8\times10^{-5}$ m$^2$/s and $1.2\times10^{-5}$ m$^2$/s respectively. Compared with heat flux from ML to sea ice, downwelling heat flux from ML into rWML is 0.87 W/m$^2$, a much lower level caused by enhanced stratification in the seasonal halocline under ML due to sea ice melt, indicating solar energy entering ML is consumed mainly by sea ice melt instead of transferring downward. Heat flux from ML into rWML changes in two phases separated by the abrupt cooling air temperature with a day lag. Upward heat flux from AW into rWML is 0.18 W/m$^2$ with no obvious changing trend, higher than previous evaluation due to larger temperature gradient caused by the existence of rWML. With the enhancing stratification in the upper ocean due to rapid sea ice retreat, upward heat flux from AW is suspected to be increasing as the surface water becomes warming and freshening in the future. Vertical heat flux from ML and AW transfers $4.43\times10^4$ J/m$^3$ and $8.39\times10^3$ J/m$^3$ heat into rWML respectively, which together comprises 36% of heat content in rWML. Working as a reservoir for heat flux, heat stored in rWML can delay the onset of sea ice freezing.

***Acknowledgement***

Data used in this research were collected during the 4th Chinese Arctic Expedition in 2010, and we are grateful to the Chinese Arctic and Antarctic Administration who provides the access to R/V *Xuelong*. Great thanks are also given to the whole expedition team who supported a lot during the in situ observation. We also want to express our gratitude to Bian Lingen and Lei Ruibo for kind providing air temperature data and GPS data.

**References**

Aagaard K, Coachman L K, Carmack E. 1981. On the halocline of the Arctic Ocean. Deep-Sea Research Part A: Oceanographic Research Papers, 28(6): 529–545

Comiso J C, Parkinson C L, Gersten R, et al. 2008. Accelerated decline in the Arctic sea ice cover. Geophysical Research Letters, 35(1): L01703

Dewey R, Muench R, Gunn J. 1999. Mixing and vertical heat flux estimates in the Arctic Eurasian Basin. Journal of Marine Systems, 21(1–4): 199–205

Fer I. 2009. Weak vertical diffusion allows maintenance of cold halocline in the central Arctic. Atmospheric and Oceanic Science Letters, 2(3): 148–152

Fowler C, Emery W J, Maslanik J. 2004. Satellite-derived evolution of Arctic sea ice age: October 1978 to March 2003. IEEE Geoscience and Remote Sensing Letters, 1(2): 71–74

Kawaguchi Y, Hutchings J K, Kikuchi T, et al. 2012. Anomalous sea-ice reduction in the Eurasian Basin of the Arctic Ocean during summer 2010. Polar Science, 6(1): 39–53

Krishfield R A, Perovich D K. 2005. Spatial and temporal variability of oceanic heat flux to the Arctic ice pack. Journal of Geophysical Research: Oceans (1978–2012), 110: C07021

Lei R B, Zhang Z H, Matero I, et al. 2012. Reflection and transmission of irradiance by snow and sea ice in the central Arctic Ocean in summer 2010. Polar Research, 31(1): 17325

Lindsay R W, Zhang J, Schweiger A, et al. 2009. Arctic sea ice retreat in 2007 follows thinning trend. Journal of Climate, 22(1): 165–176

Liu Y H, Key J R. 2014. Less winter cloud aids summer 2013 Arctic sea ice return from 2012 minimum. Environmental Research Letters, 9(4): 044002

Maykut G A, Untersteiner N. 1971. Some results from a time-dependent thermodynamic model of sea ice. Journal of Geophysical Research, 76(6): 1550–1575

Maykut G A. 1982. Large-scale heat exchange and ice production in the central Arctic. Journal of Geophysical Research: Oceans (1978–2012), 87(C10): 7971–7984

Maslanik J A, Fowler C, Stroeve J, et al. 2007. A younger, thinner Arctic ice cover: Increased potential for rapid, extensive sea-ice loss. Geophysical Research Letters, 34(24): L24501

Maslanik J, Stroeve J, Fowler C, et al. 2011. Distribution and trends in Arctic sea ice age through spring 2011. Geophysical Research Letters, 38(13): L13502

Maykut G A, McPhee M G. 1995. Solar heating of the Arctic mixed layer. Journal of Geophysical Research: Oceans (1978–2012), 100(C12): 24691–24703

McPhee M G. 1988. Analysis and prediction of short-term ice drift. Journal of Offshore Mechanics and Arctic Engineering, 110(1): 94–100

McPhee M G. 1992. Turbulent heat flux in the upper ocean under sea ice. Journal of Geophysical Research: Oceans (1978–2012), 97(C4): 5365–5379

McPhee M G. 2002. Turbulent stress at the ice/ocean interface and bottom surface hydraulic roughness during the SHEBA drift. Journal of Geophysical Research: Oceans (1978–2012), 107(C10): SHE 11-1–SHE 11-15

McPhee M G, Kikuchi T, Morison J H, et al. 2003. Ocean-to-ice heat flux at the North Pole environmental observatory. Geophysical Research Letters, 30(24): 2274

McPhee M G, Kottmeier C, Morison J H. 1999. Ocean heat flux in the central Weddell Sea during winter. Journal of Physical Oceanography, 29(6): 1166–1179

McPhee M G, Proshutinsky A, Morison J H, et al. 2009. Rapid change in freshwater content of the Arctic Ocean. Geophysical Research Letters, 36(10): L10602

Pacanowski R C, Philander S G H. 1981. Parameterization of vertical mixing in numerical models of tropical oceans. Journal of Physical Oceanography, 11(11): 1443–1451

Rudels B, Anderson L G, Jones E P. 1996. Formation and evolution of the surface mixed layer and halocline of the Arctic Ocean. Journal of Geophysical Research: Oceans (1978–2012), 101(C4): 8807–8821

Sirevaag A, de La Rosa S, Fer I, et al. 2011. Mixing, heat fluxes and heat content evolution of the Arctic Ocean mixed layer. Ocean Science Discussions, 7: 335–349

Steele M, Boyd T. 1998. Retreat of the cold halocline layer in the Arctic Ocean. Journal of Geophysical Research: Oceans (1978–2012), 103(C5): 10419–10435

Steele M, Ermold W, Zhang J L. 2008. Arctic Ocean surface warming trends over the past 100 years. Geophysical Research Letters, 35(2): L02614

Stroeve J, Serreze M, Drobot S, et al. 2008. Arctic sea ice extent plummets in 2007. Eos, Transactions American Geophysical Union, 89(2): 13–14

Thurnherr A M. 2008. How to process LADCP data with the LDEO software. version IX, 5